Electronic structure modulation in an exceptionally stable $[FeNO]_7$ nonheme nitrosyl iron spin crossover complex

Lucía Piñeiro-López,[a] Norma Ortega-Villar,[b] M. Carmen Muñoz,[c] Gábor Molnár,[d] Jordi Cirera,[e] Rafael Moreno-Esparza,[b] Víctor M. Ugalde-Saldívar,[b] Azzedine Bousseksou,[d] Eliseo Ruiz,[e] José A. Real[a*]

[a]Instituto de Ciencia Molecular (ICMol), Universidad de Valencia, 46980 Paterna, Valencia, Spain.

[b]*Facultad de Química (UNAM), Edificio B. Av. Universidad 3000, Coyoacán, México D.F. 04510, (México)*

[c]*Departamento de Física Aplicada, Universitat Politècnica de València, 46022, Valencia, Spain.*

[d]*LCC ; CNRS & Université de Toulouse (UPS, INP) ; 205 route de Narbonne, F-31077 Toulouse, France.*

[e]*Departament de Química Inorgànica and Institut de Recerca de Química Teòrica i Computacional, Universitat de Barcelona, Diagonal 645, Barcelona, 08028 Spain*

Abstract

The highly stable nitrosyl iron mononuclear complex $[Fe(bztpen)(NO)](PF_6)_2$ (**1**) (bztpen = N-benzyl-N,N',N'-tris(2-pyridylmethyl)ethylenediamine) displays an S = 1/2 ↔ S = 3/2 spin crossover behavior (SCO) [$T_{1/2}$ = 370 K, ΔH = 12.48 kJ/mol, ΔS = 33 J/K mol] stemming from strong magnetic coupling between NO radical [S =1/2] and thermally interconverted [S = 0 ↔ S = 2] ferrous spin states. The crystal structure of this robust complex has been investigated in the temperature range 120-420 K affording, for the first time, a detailed picture of how the electronic distribution of the t_{2g}-e_g orbitals modulates the structure of the $\{FeNO\}_7$ bond, providing valuable magneto-structural and spectroscopic correlations and DFT analysis.

Introduction

Heme and non-heme iron-nitrosyl complexes have been intensively investigated during the last three decades as chemical models of active Fe-NO biologically relevant sites.[1] Ferrous heme-nitrosyl complexes are Fe^{II} S = 0 low spin (LS) species with a doublet ground spin state (S = 1/2) formally originated from the NO ligand.[2] Ferric heme-nitrosyl complexes derive from the LS state of Fe^{III} (S = 1/2) and afford singlet ground spin state (S = 0) species.[2] In contrast, nonheme iron-nitrosyl complexes can exist either in the S = 3/2 or the S = 1/2 spin states depending on the ancillary ligands.[3] Interestingly, a small number of nonheme iron-nitrosyl complexes show S = 3/2 ↔ S = 1/2 spin crossover (SCO) behavior. Six of them are penta-coordinate complexes formulated [FeL(NO)] (with L = salen,[4] salphen,[5] (L_1)[6], (L_{1a}),[6] (L_2)[7]), and [Fe(TMC)(NO)]$(BF_4)_2$[8], while the remaining are the hexa-coordinate complexes $[FeL_3(NO)(CH_3OH)]$,[7] $[FeL_4(NO)(CH_3OH)]$,[7] and $[FeL_{pr}(NO)]$,[9] (see Scheme I).

In the Enemark and Feltham systematization of the M-NO bonding, nonheme iron-nitrosyl complexes are considered $\{FeNO\}_7$ species, where 7 is the total number of electrons in the Fe d and NO π* orbitals.[10] The radical character of the non-innocent NO ligand and close energetic proximity to the Fe d-orbitals determine the essence of the bonding in the $\{FeNO\}_7$ moiety. Depending on the d-π* energy difference, different electronic structures have been envisaged. However, the substantial degree of covalence involved in the {FeNO} unit makes difficult an unambiguous assignation of specific oxidation and ground spin states.[11] For example, from an analysis of the Fe K-edge X-ray absorption spectroscopy of a series of S = 3/2 non-heme iron nitrosyl complexes, which included [Fe(salen)(NO)], Solomon et al. concluded that the S = 3/2 $\{FeNO\}_7$ species are more precisely specified as a HS (S = 5/2) ferric center antiferromagnetically coupled with the NO^- (S = 1) anion.[12] Based on a combination of electron spin resonance and Mössbauer spectroscopies and DFT methods, Wieghardt et al. reached the same conclusion for the SCO complex $[FeL_{pr}(NO)]$ in the S = 3/2 state.[9] Furthermore, these authors proposed for the S = 1/2 spin state a LS (S = 0) ferrous center coupled with $NO^{\cdot}$ (S = 1/2). The latter conclusion has recently been supported by Salomon et al from sulfur-K-edge X-ray absorption spectroscopy and DFT studies on two model complexes that contains sulfur ligands.[13] Thus, for $\{FeNO\}_7$ SCO species the observed S = 3/2 ↔ S = 1/2 equilibrium could be more precisely described as a valence tautomerism process.[9] In contrast, DFT calculations of the Mössbauer parameters of the [Fe(salen)(NO)] SCO complex and other studies on the isopenicillin N synthase, Oldfield et al. have concluded that the investigated S = 3/2 $[FeNO]_7$ species can be described as a HS (S = 2)

ferrous Fe^{II} antiferromagnetically coupled with NO (S = ½).[14] The same conclusion was drawn from a recent spectroscopic and computational study of a nonheme iron nitrosyl center in a biosynthetic model of nitric oxide reductase.[15]

In previous studies we investigated the suitability of the pentadentate N-benzyl-N,N',N'-tris(2-pyridylmethyl)ethylenediamine (bztpen) ligand in the synthesis of new $\{[Fe^{II,III}(bztpen)]_xL\}(PF_6)_y$ spin crossover (SCO) complexes with the sixth coordination occupied by suitable ancillary monodentate L- ligands such as dicyanamide (Fe^{II}, x = 2, y 3)[16] or alkoxydes (Fe^{III}, x = 1, y = 2).[17] In addition Schindler et al. have compared the stability of the $[Fe(bztpen)(NO)]^{2+}$ cation in solution with respect to that of the homologous Fe^{III} peroxo and hydroperoxo complexes, and the crystal structure of the triflate derivative $[Fe(bztpen)(NO)](CF_3SO_3)_2$ was succinctly described in this study.[18]

Following our research line and in principle motivated by the study of the interplay between the SCO phenomenon and strong magnetic coupling, here we report the synthesis and characterization of the complex $[Fe(bztpen)(NO)](PF_6)_2$ (**1**) in the solid state. **1** is a new non-heme $[FeNO]^7$ species displaying a SCO equilibrium that extends beyond 400 K. Facilitated by the extraordinary robustness of the single crystals, a detailed single crystal analysis carried out in the temperature range 120-420 K shows the adaptability of the NO molecule to the change of spin-state in the Fe center. Furthermore, multi-temperature EPR, Mössbauer, IR, Raman and UV-Vis spectroscopies as well as theoretical calculations have been carried out to clarify the nature of the observed S = 3/2 ↔ S = 1/2 equilibrium.

Results and discussion

Synthesis.

When NO(g) is bubbled, in anaerobic conditions, into a saturated pale-yellow methanolic solution of $[Fe^{II}(bztpen)(MeOH)]^{2+}$ (ca. $3\cdot10^{-3}$ M) a deep-purple solution is instantaneously formed followed by rapid and quantitative precipitation of a microcrystalline brown-purple solid **1**. Starting from diluted solutions ($\geq 9\cdot10^{-4}$ M) of $[Fe^{II}(bztpen)(MeOH)]^{2+}$ and following the same procedure single crystals of **1** were obtained in a few days.

Magnetic Properties

The thermal dependence of the $\chi_M T$ product in the interval of temperatures 2-400 K for **1** is shown in Figure 1 (χ_M is the magnetic susceptibility and T temperature). At 400 K $\chi_M T$ is 1.35 cm^3

K mol^{-1} and continuously decreases with cooling until 0.38 cm^3 K mol^{-1} at ca 150 K. Below this temperature $\chi_M T$ remains practically constant down to 15 K. In the temperature range 15-2 K a quite small decrease denotes the onset of very weak intermolecular antiferromagnetic interactions. The $\chi_M T$ = 0.38 cm^3 K mol^{-1} is consistent with an S = 1/2 ground state with g = 2.01. The increase of $\chi_M T$ above 150 K is consistent with a gradual SCO. Assuming that the SCO takes place between the LS (S = 0) and HS (S = 2) spin states of an Fe^{II} strongly antiferromagnetically coupled to the S = 1/2 state of NO, the SCO can be considered to occur in an effective way between the resulting S = 1/2 and 3/2 states. In this framework ca. 54.3% of the molecules are in the S = 3/2 state at 400 K. According to previous work,[9,13] an equivalent scenario could involve occurrence of valence tautomerism in the Fe-NO moiety. This would afford the strong antiferromagnetically coupled S = 5/2 (Fe^{III}) and S = 1 (NO$^-$) spin states and the uncoupled S = 0 (Fe^{II}) and S = 1/2 (NO) spin states.

In order to evaluate the thermodynamic parameters associated with the spin change we have considered that $\chi_M T$ can be expressed as follows:

$$\chi_M T^{obs} = (\chi_M T)_{NO} \cdot (1 - f) + (\chi_M T)_{Fe-NO} \cdot f \quad (1)$$

and

$$f = 1/\{1 + exp[(\Delta H/R) \cdot (1/T - 1/T_{1/2})]\} \quad (2)$$

where $(\chi_M T)_{NO}$ is the $\chi_M T$ value at low temperatures due to the presence of the radical NO (S = 1/2) and Fe^{II} (S = 0) , $(\chi_M T)_{Fe\text{-}NO}$ is the expression of a dinuclear species derived from the Hamiltonian $\mathbf{H} = -J\,\mathbf{S}_a\mathbf{S}_b$ with S_a = 1/2 or 1 and S_b = 2 or 5/2 species, respectively,[19a] f is the molar fraction of the HS species expressed by the theory of regular solutions in the form given by Slichter and Drickamer.[19b] In eq. 2, ΔH is the enthalpy variation, R is the universal constant of gases and $T_{1/2}$ is the temperature at which HS and LS species are present at 50% ($\Delta G = 0$). Given the expected large magnitude of the magnetic coupling constant (J), it is safe to consider that only the S = 3/2 state plays an effective role in $(\chi_M T)_{Fe\text{-}NO}$. A least squares fit procedure, which minimizes the function $R_{min} = \Sigma(\chi_M T_{obs} - \chi_M T_{calcd})^2 / \Sigma(\chi_M T_{obs})^2$, leads as adjustable parameters $g_{3/2}$ = 2.15, ΔH = 12.48 kJ/mol, $T_{1/2}$ = 377.6 K and $R_{min} = 7 \cdot 10^{-5}$. The total entropy variation is given by $\Delta S = \Delta H/T_{1/2}$ = 33 J/Kmol.

The excellent agreement between calculated and experimental data supports the assumption of synchronous reversible spin-state conversion and strong antiferromagnetic coupling between Fe^{II} and NO. This strong antiferromagnetic coupling is in line with the magnitude of the J parameter estimated from our DFT calculations for **1** (vide infra) and those reported by Wieghardt and co-workers for the complex Tp*Co(NO) [Tp* = hydro-tris(3,5-Me$_2$-pyrazolyl)borate].[20] The ΔS value

is found clearly smaller than typically observed for Fe^{II} SCO complexes[21] and in the lower limit observed for Fe^{III} SCO complexes[22] but consistent with a S = 1/2 ↔ S = 3/2 transformation.[23]

It is worth mentioning the similarities between the magnetic behavior of **1** and that reported by Krügger and co-workers for [Fe(L-N_4Me_2)(bian^{1-})](ClO_4), where L-N_4Me_2 and bian^{1-} are, respectively, N,N'-dimethyl-2,11-diaza[3.3]-(2,6)pyridinophane and the radical anion of N,N'-diphenylacenaphtene-1,2-diimine.[24] In the temperature interval 22-240 K, this compound displays a $\chi_M T$ value, 0.37 cm^3 K mol^{-1}, consistent with an S = 1/2 ground state. Then upon heating $\chi_M T$ smoothly increases reaching a value of 0.75 cm^3 K mol^{-1} at 380 K indicating partial population of the S = 3/2 state. Based on the magnetic properties, EPR and Mössbauer spectra Krügger et al. concluded that the observed behavior corresponds to a combined effect of strong antiferromagnetic coupling between the radical ligand bian^{1-} and the Fe^{II} ion switching between the S = 0 and S = 2 states. Much weaker magnetic coupling was reported for a series of five-coordinate halido and pseudohalido-bis(o-iminobenzosemiquinonato)iron(III) complexes that undergo SCO between the effective spin states S = 3/2 and S = 1/2.[25]

Spectroscopic Characterization of 1

EPR spectra. The X-band EPR solid-state spectra of **1** collected at 4 K and 300 K is shown in Figure 2a. At 4 K the spectrum is characterized by a sharp signal centered at g = 2.02 which becomes wider without moving significantly (g = 2.05) at 300 K where, according to the magnetic properties, ca 30% of the molecules are in the S = 3/2 state. This EPR is reminiscent of that reported for the classical SCO nitrosyl compound [Fe(salen)(NO)] for which no signal at g ≈ 4 characteristic of the S = 3/2 state is observed, which was considered consistent with an electron essentially residing in the NO molecule.[26] Similarly, no observation of the S = 3/2 signal was reported for the SCO complex [FeL_{pr}(NO)].[9] In contrast the EPR spectrum of the non-heme HS iron(II)-nitrosyl model complex [Fe(BMPA-Pr)(NO)(Cl)][27] (BMPA-Pr = N-propanoate- N, N-bis(2-pyridylmethyl)amine)] is characterized by a dominant signal at g ≈ 4 attributable to the S = 3/2 state.

Mössbauer spectra. ^{57}Fe Mössbauer spectra at 80 K and 293 K for **1** are shown in Figure 2b. The low intensity of the 293 K spectrum discouraged us from recording Mössbauer spectra at higher temperatures since it was expected relatively poor signal to noise ratio. The fitted spectral parameters (assuming Lorenzian line-shapes) are given in Table S1. The 80 K spectrum can be assigned to a low spin ferrous or ferric species (not distinguishable by Mössbauer) with isomer shift δ = 0.306(5) mms^{-1} and quadrupole splitting ΔE_Q = 0.523(9) mms^{-1}. Detection of only one doublet

at 293 K, δ = 0.295(4) mms^{-1} and ΔE_Q = 0.590(8) mms^{-1}, is consistent with fast spin-state interconversion rate compared to the time scale of Mossbauer spectroscopy leading to an averaged spectrum. This is also supported by the unusual and almost insignificant thermal variation of the spectrum parameters ΔE_Q and δ. A similar situation was reported for the nitrosyl SCO complexes [Fe(TMC)NO](BF$_4$)$_2$,[8] [FeL$_1$(NO)][28] and [FeL$_{1a}$(NO)][28] (see Scheme I) and for the aforementioned SCO complex [Fe(L-N$_4$Me$_2$)(bian$_{1-}$)](ClO$_4$)$_2$[4]. In contrast, the characteristic signals of both spin states were observed for [Fe(salen)(NO)],[29] [Fe(salphen)(NO)][5] and [Fe(L$_{pr}$)(NO)].[9] All these Fe^{II} SCO nitrosyl complexes, included **1**, display δ values of the same order of magnitude, found in the interval 0.3- 0.5 mms^{-1}.

Visible spectra. Figure 2c displays the reflectance spectrum of **1** at 293 K, where the relative population of Fe^{II} LS and HS states is estimated to be LS:HS $\approx$ 73:27. The spectrum is characterized by three absorption bands centered at ca 400 nm, 555 nm and 730 nm. If one assumes that the three maxima are predominantly of d-d character they could be tentatively ascribed to the $^1A\rightarrow{}^1T_2$, $^1A\rightarrow{}^1T_1$ and $^5T\rightarrow{}^5E$, respectively.[30] A similar spectrum has been reported for the S = 1/2 {FeNO}^{7} complex trans-[(cyclam)Fe^{II}(NO)Cl](ClO$_4$) in acetonitrile solution with bands at 398 nm (ε = 300 M^{-1} cm^{-1}) and 560 nm (ε = 145 M^{-1} cm^{-1}) reasonably ascribed to the Fe^{II} in the LS state since they disappear after one-electron oxidation suggesting a metal-centered process.[31]

Interestingly, **1** displays thermochromism in the temperature interval 175-425 K. Upon heating the brown-violet color of the crystal becomes pale (see Figure S1). This color change is primarily related to the bleaching of the 555 nm absorption, which starts above ca. 200 K to be completed to ~80 % at 425 K (inset Figure 2c). This assignment is supported not only by the weak absorption coefficients, ~70 cm^{-1} and ~3 cm^{-1}, associated with the 555 and 730 nm peaks, respectively, but also by the remarkably good correlation between the temperature dependence of the intensity of the 555 nm band and the magnetic behavior of **1** shown in Figure 3. It is worth mentioning at this point that the thermochromism observed upon $^1A \leftrightarrow {}^5T$ spin-state change in Fe^{II} SCO complexes, particularly marked in absence of strong CT bands, is associated with the $^1A\rightarrow{}^1T_1$ transition.

Vibrational spectra. Variable temperature, single-crystal Raman spectra were acquired using both 532 nm and 633 nm laser excitations. Representative spectra are shown in Figure 4a. The NO stretching mode, ν_{NO}, undergoes a remarkable shift from 1789 cm^{-1} to 1684 cm^{-1} (for both excitation wavelengths) when going from 400 K to 100 K. These characteristic vibrational modes can be clearly associated with the S = 3/2 and S = 1/2 states, respectively, since they co-exist (in different proportions) in the temperature interval where the conversion between these two magnetic states takes place. Indeed, as shown in Figure 3 the relative intensity of these modes

follows reasonably well the magnetic changes (a better correlation would be rather fortuitous as the intensity of Raman modes is not directly proportional to the population of the two electronic states).

The temperature dependent, single-crystal IR absorption spectra (Figure 4b) confirm well the Raman data. At 473 K a broad absorption band is observed at around ca. 1780 cm^{-1} as well as its overtone around 3543 cm^{-1}, which can be attributed to the ν_{NO} mode of the complex in the S = 3/2 state. At 123 K these bands disappear and an ill-resolved shoulder, assigned to the ν_{NO} mode in the S = 1/2 state, appears at around 1670 cm^{-1}. This assignment is further substantiated by the observation of the overtone of this mode at 3337 cm^{-1}. Similar to the Raman spectra the NO stretching peaks (fundamental as well as overtone) associated with the S = 3/2 state are much broader than their S = 1/2 state counterparts, which may indicate a disorder in the former. These results agree reasonably well with the corresponding ν_{NO} IR modes reported for [Fe(salen)(NO)] 1712 (S = 3/2) and 1630 (S = 1/2) cm^{-1}.[4] Nevertheless, the shift of the ν_{NO} mode is ca. 20% larger for **1** most likely reflecting the distinct chemical nature of the ligands salen and bztpen and coordination number of both complexes.

In the case of the IR absorption spectra the temperature dependence of the peak intensities is considerably altered by heating due to the IR probe beam. For this reason, the quantitative correlation of IR absorbance changes with the magnetic data was not possible. It is important to note, however, that the spin conversion at low temperatures is fully complete since the characteristic ν_{NO} IR absorption bands (and also Raman peaks) of the high temperature form disappear completely below ca. 200 K. Due to the weak spectral intensities above 400 K it is more difficult to conclude about the completeness of the transition at high temperatures, but we can note that no residual fraction is observed in the IR spectra at 473 K, indicating a nearly complete transition (Figure 4b).

Besides the ν_{NO} stretching mode, several other spectral changes are observed in the Raman spectra. At high temperature, where the S = 3/2 state is significantly populated, a medium band dominates over 503 cm^{-1} the Raman spectrum of **1**. Interestingly, the intensity of this peak decreases upon cooling down to 100 K at expense of a new peak centered at 603 cm^{-1}. According to previous reports it is reasonable to tentatively assign the 603 cm^{-1} and 501 cm^{-1} frequencies to coupled Fe-NO stretching and FeNO bending modes (*vide infra*) in the S = 1/2 and S = 3/2 states, respectively.[3,32-35]

Structure of 1

The crystal structure of the title compound was investigated at 120 K, 200 K, 250 K, 275 K, 300 K, 340 K, 380 K, 400 K and 420 K on the same single crystal. The crystal belongs to the orthorhombic *Pbca* space group in the range of temperatures investigated. Selected crystallographic data are gathered in Table 1. The molecular structure is displayed in Figure 5 (left) together with the atom-numbering scheme and representative bond lengths and angles are collected in Table 2. The iron atom is in a distorted octahedral [FeN_6] environment defined by five nitrogen atoms belonging to the pentadentate bztpen ligand and the nitrogen atom of the nitroxyl group. Two PF_6^- anions balance the charge of the $[Fe(bztpen)(NO)]^{2+}$ cation. The *bztpen* ligand coordinates the Fe, defining a distorted square pyramid in which the N(2) atom lies on the axial apex. The opposite apex is occupied by the N(6) of the NO molecule. The N(2) atom is in the center of a tripod whose arms are defined by two picolylamine-type moieties [N(2)–C(7)–C(8)–N(3) and N(2)–C(6)–C(5)–N(1)] and an ethylenediamine-type moiety [N(2)–C(13)–C(14)–N(4)]. These arms are anchored to the Fe through the atoms N(3), N(1), and N(4), respectively. An additional picolylamine-type arm, [N(4)-C(15)-C(16)-N(5)], originates at the N(4) atom and coordinates the remaining equatorial position of the Fe center through N(5).

The average Fe–N bond length of the Fe*bztpen* moiety, $\langle FeN_{bztpen}\rangle_{av}$, gradually increases with increasing temperature from 2.031 (120 K) Å until 2.135 (420 K) involving a total variation of practically 0.1 Å. Consistently, the sum of deviations from the ideal octahedron of the 12 "cis" N–Fe–N angles ($\Sigma = \sum_{i=1}^{12}|\theta_i - 90|$) shows that the coordination center is strongly distorted at 120 K with $\sum$ = 60.9º and this distortion increases as temperature increases until reaching a value of 76.8º at 420 K. In contrast, the trigonal distortion parameter, defined as $\Phi = \sum_{i=1}^{24}(|\phi_i - 60|)/24$ (there are 24 ϕ_i angles generated by superposition of 4 pairs of opposite triangular faces of an octahedron; ϕ_i □□□6□º□□□□□□□□□gular octahedron), is small at 120 K (Φ = 4.4º) and increases up to 5.5º at 420 K. The Fe-NO bond length (Fe-N(6)) displays a very small increase from 1.733(3) to 1.751(7) Å making slightly less pronounced the overall change of the average [FeN_6] bond length, $\Delta R(\langle Fe\text{-}N_6\rangle)$ = 0.089 Å (Table 2). The thermal dependence of $\langle Fe\text{-}N_6\rangle$ shows an excellent correlation with the thermal dependence of $\chi_M T$ (Figure 6a). As mentioned above ca. 54.4% of the cations populate the S = 3/2 state at 400 K. Extrapolation of this population to 100% gives a total variation $\Delta R(Fe\text{-}N_{av}) \approx 0.145$ Å, which is ca 27% shorter than usually observed for an Fe^{II} center undergoing complete SCO behavior (0.2 Å). In part, this is mitigated by the small variation observed for the Fe-N(6)-O bond length. This small variation of the Fe-N(6)-O bond length contrasts with the ca. 100 cm^{-1} shift of the $\nu_{Fe\text{-}NO}$ mode upon spin state change.

The strong covalence of the Fe-NO bond is reflected specially on the thermal dependence of the N(6)-O bond length and the Fe-N-O tilt angle (Table 2). Upon heating from 120 K to 420 K, the N-O bond length gradually decreases from 1.170(4) Å to 1.099(10) Å. This significant decrease of 0.071 Å results from gradual population of the S =3/2. At low-temperatures, where the S = 1/2 state is fully populated, the electronic repulsion in the filled t_{2g}-Fe orbitals facilitates some electron density delocalization into the π*-NO orbitals through π-back-bonding mechanism inducing lengthening of the N-O bond. In contrast, at high temperatures, where the S = 3/2 state is populated, the partial promotion of the electrons from the t_{2g} orbitals to the e_g orbitals considerably reduces the electron density delocalization into the π*-NO orbitals inducing shortening of the N-O bond.

The Fe-N-O(1) angle increases from 144.0(3)º to 157.9(10)º when moving from 120 K to 420 K. This thermal dependence clearly follows the thermal dependence of the Fe-N_{av} bond length and $\chi_M T$ (Figure 6b). Hence, the Fe-N-O(1) angle also changes with the population of the S = 3/2 and S = 1/2 molecular states, each one characterized by a different FeNO bond angles. Extrapolation of this variation to 100% S = 3/2 state population predicts an increase of the Fe-N-O angle up to 167°.

The only known crystal structure of a $\{FeNO\}_7$ SCO system in the pure S = 1/2 and S = 3/2 states were reported for [Fe(salen)(NO)].[36] For this compound, the average Fe-N-O angle changes from 127° in the S =1/2 state to 147° in the S = 3/2 state. Although the magnitude of these angles is markely smaller than found for **1** (ca. 20º), the change of 20° is very close to the 23º variation estimated upon complete SCO in **1**. Furthermore, the average variation of the bond lengths in the FeN_2O_2 core, 0.040Å, is ca. 50% smaller than observed for **1** at 420 K or ca 73% smaller than expected for a complete conversion in **1**. As mentioned above this large difference could be accounted for the distinct chemical nature of the ligands and coordination number and geometry of both complexes.

A perspective of the crystal packing in the [100] direction is displayed in Figure 5 (right). This perspective shows an apparent organization of the cationic species by pairs that indeed correspond to the two first members of infinite supramolecular zig-zag “chains” running along [100] direction with shortest Fe···Fe distances ranging in the interval 9.4237(8)-9.5697(10) Å in the temperature range 120-400 K. There are C···C intermolecular contacts between in the infinite supramolecular chains, namely C(23)···C(11) = 3.651(14) Å, C(26)···C(2) = 3.601(14) Å, C(24)···C(10) = 3.645(14) Å, C(25)···C(1) = 3.643(14) Å and C(24)···C(11) = 3.587(14) Å at 120 K (see Figure S2). Furthermore, in the LT crystal packing the cationic molecules interact directly with each other through weak C···C intermolecular contacts defining a three-dimensional network. Most of these contacts are in the interval 3.6-3.7 Å. These interactions are reinforced by a number of C···F

cation−anion contacts. Table S2 gathers the intermolecular distances smaller than the sum of the van der Waals radii C···C and C···F.

Electronic structure modeling

The $[Fe(bztpen)(NO)]^{2+}$ molecule has been fully optimized (see Computational details section) in the different possible spin topologies, this is, Fe^{II}-NO and Fe^{III}-NO^{-} in both ferromagnetic and antiferromagnetic schemes between the paramagnetic centers, and also allowing the iron centers to be in the high- or low-spin state. A complete list of atomic Cartesian coordinates for the optimized structures, as well as its energies can be found in the Supporting Information (Table S3). When optimizing the systems in the Fe^{III}-NO^{-} motif, an electron transfer from the NO^{-} ligand to the Fe^{III} center is always observed, thus, reducing the metal to Fe^{II} and generating an NO radical. This is in line with the conclusion raised by Solomon and coworkers which states that six coordinate strong ligand field $\{FeNO\}^{7}$ complexes and specially those with a strong axial donor atom in trans to the NO molecule, as is the case of **1**, destabilizes the Fe^{III}-NO^{-} configuration in of favor the Fe^{II}-$NO^{\cdot}$ configuration.[37] The optimized bond lengths and angles for the $[Fe(bztpen)(NO)]^{2+}$ molecule in the S = 1/2 and S = 3/2 states are in good agreement with the corresponding experimental data at 120 K (LS state) and extrapolated to 100% populated S = 3/2 state (see Table 2). The most relevant discrepancy corresponds to the much larger experimental variation of the N(6)-O bond length with respect to the calculated one.

The corresponding vibrational analysis was also done to ensure the minimum nature of the optimized structures. It is worth mentioning at this point that the calculated $\nu_{NO}(1/2)$ = 1774.2 cm^{-1} and $\nu_{NO}(3/2)$ = 1837.4 cm^{-1} are respectively ca. 100 and 56 cm^{-1} larger than the corresponding experimental but are within the normal limits found for DFT calculations (about 5%). In contrast, the calculated $\nu_{Fe\text{-}NO}(3/2)$ = 501 cm^{-1} is about 5% smaller than the experimental one. The most important difference corresponds to the calculated $\nu_{Fe\text{-}NO}(1/2)$ = 494.2 cm^{-1} which is ca. 18% smaller than the experimental value.

Significant differences in the Fe-NO bonding interactions can be observed as a function of the metal spin-state when analyzing the electronic structure of the molecule in terms of the relevant molecular orbitals. In the low-spin state (S = 1/2) the occupied orbitals include the Fe-NO bonding d_{xz} and d_{yz} pair of orbitals and the non-bonding d_{xy} orbital. The d_{x2-y2} and d_{z2} orbitals are strongly antibonding with the pentadentate ligand and the NO group, but remain unoccupied. Both d_{xz} and d_{yz} are involved in bonding interactions with the π_x and π_y orbitals of the NO ligand respectively, being the unpaired electron located in the d_{yz}-π_y orbital. With the transition to the high-spin state

(S=3/2), the d_{x2-y2} and d_{z2} orbitals remain strongly antibonding but are now single-occupied, while the Fe-NO bonding interactions are strongly reduced, and the d_{xz} and d_{yz} d-based MOs turn now into formally non-bonding, although a certain antibonding character with the oxygen p_x and p_y orbitals respectively can be observed. This situation leads to an enlargement of the Fe-NO bond length upon spin-crossover of around 0.02 Å. A molecular orbital diagram including de relevant d-based MOs is included in the ESI (Figure S3).

The electronic structures for each spin state correspond with a low-spin Fe^{II} (d_6, S = 0) and a high-spin Fe^{II} (d_6, S = 2) antiferromagnetically coupled with an NO radical (S = 1/2), thus leading to the observed spin-states, S = 1/2 and S = 3/2, respectively. The corresponding plot of the spin density shows (see Figure 7) that, indeed, for the S = 1/2 spin-state the electron is mainly located on the NO ligand. In the metal, there is a blue region due to the delocalization of the spin density of the radical in the orbital oriented towards the NO group while the red region correspond to some spin polarization mechanism in the orbitals without overlap with the NO orbitals bearing the unpaired electron. The S = 3/2 spin-state has spin density in both, the metal center and the NO ligand with opposite signs and the N atoms of the bztpen ligand have the same sign than the metal due to the large spin delocalization (strong mixing of the orbitals with unpaired electrons of the iron center). To calculate the magnetic exchange constant, the high-spin Fe^{II} (d_6, S = 2) ferromagnetically coupled to the NO radical (S = 1/2) solution was also calculated. This system has a total spin-state of S = 5/2, and using the expression in eq. 3 together with the electronic energy of the S = 3/2 spin-state, a value of J_{calc} = -2843 cm^{-1} is obtained, which is in the right range and comparable with the calculated value for complex Tp*Co(NO) (Tp* = hydro-tris(3,5-Me2 -pyrazolyl)borate).[20]

To model the spin transition between the S = 1/2 and S = 3/2 states one must first calculate the corresponding temperature dependence change in the free energy associated with this process. That can be achieved by correcting the corresponding electronic energies for each spin state with the vibrational contribution using the harmonic approximation.[4, 6] Thus, at each temperature we can compute the corresponding $\Delta G(T)$, and from this thermochemical quantity extract relative populations for each spin-state (see Supporting Information for methodological details). In Figure 8 we report the magnetic behavior of **1** in the temperature range 0 to 600 K compared with the experimental data. As can be seen, the calculations nicely agree with the experimental data, although the computed equilibrium transition temperature ($T_{1/2calc}$ = 546.8 K), at which $\Delta G(T) = 0$, is significantly shifted towards higher values with respect to the experimental value ($T_{1/2exp}$ = 378 K). This circumstance has been previously reported for other Fe^{II} spin-crossover mononuclear complexes, and corresponds to an error of 0.33 kcal/mol, similar to previously reported

calculations, and can be explained on the basis of the amount of exact exchange Hartree-Fock mixed into the TPSSh functional. [4, 5]

Por favor, clarificar las referencias marcadas en Amarillo 4, 5, 6

Concluding remarks

Nitroxyliron complexes exhibiting spin crossover properties (SCO) are scarce $\{FeNO\}_7$ species that in virtue of strong magnetic coupling invariably display S = 3/2 ↔ S = 1/2 spin state conversion. The large thermal stability of **1** has allowed, for the first time, to describe in a precise way how the changes in electronic distribution of the t_{2g}-e_g orbitals due to SCO modulates the structure of the $\{FeNO\}_7$ species providing valuable magneto-structural and spectroscopic correlations.

The magnetic properties of **1** show the occurrence of a very gradual SCO, which extends far beyond 400 K where the population of the HS species is estimated to be 54.4%. The narrow EPR signal at g ≈ 2 suggests that the unpaired electron essentially resides in the π* orbitals of NO in the S = 1/2 state. This signal widens at room temperature but remains approximately at the same g value. No feature at g ≈ 4 associated with the S = 3/2 state is observed despite it is ca. 30% populated at 300 K. The Mössbauer spectra of **1** at 80 and 293 K is consistent with the occurrence of fast spin-state interconversion rate with poor temperature dependent isomer shift parameter in the temperature interval 80-293 K, a fact that strongly limits the characterization of the electronic structure of the $\{FeNO\}_7$ moiety from this technique. The room temperature visible spectrum of **1** is consistent with the presence of bands characteristic of the Fe^{II} in the LS state. Furthermore, the thermal variation of the 555 nm band tentatively attributed to the $^1A_1 \rightarrow {}^1T_1$ absorption and the concomitant change of color of the complex are reminiscent of Fe^{II} complexes which exhibit S = 0↔S = 2 spin state change. The thermal dependence of the Raman and IR spectra have enabled to characterize the stretching ν_{NO} and $\nu_{Fe\text{-}NO}$ modes in the S = 3/2 and S = 1/2 states. All these changes in magnetism and visible, Raman and IR spectra correlate quite well with the structural changes observed in the coordination $[FeN_6]$ core of **1**, namely, average Fe-N bonds and angles including the tilt Fe-N-O angle and the N-O bond length. Furthermore, the DFT calculations reproduce reasonably well the structure of **1** in the LS and HS states and support the idea that the pentadentate strong ligand field ligand bztpen stabilizes the Fe^{II} and the NO·. Consequently, the S = 3/2↔S = 1/2 spin equilibrium accommodates well with the concurrence of an S = 2↔S = 0 spin equilibrium in the Fe^{II} and strong magnetic coupling with the radical NO.

Experimental

General

Variable-temperature magnetic susceptibility data were recorded for single crystals and microcrystalline samples of **1** and **2** at a scanning rate of 1 K/min with a Quantum Design MPMS2 SQUID susceptometer equipped with a 7 T magnet, operating at 1 T and at temperatures 2–400 K. Experimental susceptibilities were corrected from diamagnetism of the constituent atoms by the use of Pascal's constants. UV-VIS diffuse reflectance spectra of the microcrystalline powder of **1** was acquired at room temperature in the 328-1000 nm spectral range using a Lambda35 spectrophotometer (Perkin Elmer) equipped with an integrating sphere. Variable temperature absorbance data were obtained in the 480 – 680 nm range on a flat single crystal of ca. 90 □m thickness in transmission mode using an Olympus BX51 microscope, which was fiber coupled to a CCD spectrometer (BWTek). Temperature-dependent, polarized Raman spectra of oriented single crystals were recorded between 100-2000 cm^{-1} using a LabramHR (Horiba) Raman microspectrometer (resolution ca. 3 cm^{-1}) using 633 nm and 532 nm laser excitations. Laser light was focused on the sample and the scattered light was collected using the same x50 objective (0.5 numerical aperture). Laser-induced heating effects were carefully checked by monitoring at room temperature the intensity ratio of the ν(NO) modes as a function of the laser intensity and found practically negligible below ca. 0.1 mW, which was then used in the experiments. Polarization behaviour of the scattered photons vs. the polarization state of the incident laser and the crystal orientation was also studied. As expected, the ν(NO) modes are strongly polarized and the highest intensity spectra were obtained in the configuration -z(yy)z (Porto's notation). Non-polarized infrared absorption spectra as a function of temperature were collected between 600-4000 cm^{-1} in transmission mode on a flat single crystal of ca. 30 μm thickness using a Spectrum Frontier FTIR instrument (Perkin Elmer) coupled to a Spotlight-400 microscope. To acquire variable temperature vibrational and electronic spectra the same liquid nitrogen microscopy cryostage (THMS-600, Linkam Scientific) was used with either glass or CdSe windows. ^{57}Fe Mössbauer spectra were recorded using a conventional constant-acceleration-type spectrometer equipped with a 50 mCi ^{57}Co source and a flow-type, liquid-nitrogen cryostat. Spectra of the powder samples were recorded at 80 K and 293 K. Least-squares fittings of the Mössbauer spectra have been carried out with the assumption of Lorentzian line shapes using the Recoil software package. Isomer shift values are given relative to metallic iron at room temperature. Elemental analysis (C, H, N) were performed by the Centro de Microanálisis Elemental de la Universidad Complutense de Madrid (Spain) using a LECO CHNS-932 analyzer.

Variable-temperature EPR spectra were recorded on microcrystalline samples using a Bruker ELEXYS E580 spectrometer equipped with Bruker standard resonators for the X and Q bands. Data were collected in the 20-9980.0 G field range at 4 K (frequency = 9.472 GHz, power = 0.0063 mW, power attenuation = 45.0 dB, modulation frequency = 100.00 kHz, modulation amplitude = 1.000 G, gain = 60 dB) and at 300 K (frequency = 9.472 GHz, power = 62.84 mW, power attenuation = 5.0 dB, modulation frequency = 100.00 kHz, modulation amplitude = 1.000 G, gain = 60 dB).

Single crystal X-ray measurements

Single-crystal X-ray data of **1** were collected on an Oxford Diffraction Supernova single crystal diffractometer using MoKα radiation (λ = 0.71073 Å). A data scaling and empirical absorption correction was performed. The structures were solved by direct methods using SHELXS-97 and refined by full-matrix least squares on F_2 using SHELXL-97.[38] Non-hydrogen atoms were refined anisotropically. Hydrogen atoms were geometrically placed (riding model) and assigned fixed isotropic displacement parameters. CCDC xxxxx.

Computational details

All Density Functional Theory (DFT) calculations were carried out using the Gaussian 09[39] (revision D.01) electronic structure package with a tight convergence criterion (10^{-8} a.u. in the energy) for the density matrix elements, using the hybrid-meta GGA functional TPSSh.[40,41] This functional has been previously used with success in the modeling of accurate thermochemical quantities for several mononuclear and dinuclear Fe^{II} spin-crossover systems.[42-45] The fully optimized contracted triple-ζ all electron Gaussian basis set with polarization functions developed by Ahlrichs and co-workers was employed for all the elements in the molecule.[46] The different spin topologies were modeled using the fragments option, which allows the definition of specific charges and electronic structures for the metal and for the different ligands. To calculate the exchange interaction,[47,48] a phenomenological Heisenberg−Dirac−van Vleck Hamiltonian (HDVV) was used, excluding the terms relating to magnetic anisotropy, to describe the exchange coupling:

$$\hat{H} = - J_{ab} \hat{S}_a \hat{S}_b \qquad [3]$$

where $\hat{S}_a$ and $\hat{S}_b$ are the spin operators of the different paramagnetic centers. The J_{ab} parameter is the pairwise coupling constant between the paramagnetic centers of the molecule.

Materials

Synthesis of 1. Samples of **1** essentially constituted of single crystals were obtained in a very good yield (*ca* 90%) bubbling nitric oxide for 10 min through diluted solutions of [Fe(*bztpen*)CH_3CN]$(PF_6)_2$[49] (approximately 30 mg 0.037 mmol in 40 mL of MeOH). The final violet solution was kept under argon in repose and closed for three days to lead the precipitation of single crystals of appropriate size for single crystal X-ray diffraction The crystals melt with decomposition at ca. 480 K. Elemental analysis: Calculated for $C_{27}H_{29}F_{12}FeN_6OP_2$; C, 40.57; H, 3.66; N, 10.51. Found: C, 39.81; H, 3.73; N, 10.39.

Acknowledgements

The research reported here was supported by the Spanish Ministerio de Economía y Competitividad (MINECO) and FEDER funds (CTQ2013-46275-P) and Generalitat Valenciana (PROMETEO/2012/049). L.P.L. thanks the Generalitat Valenciana and the Universidad de Valencia for a predoctoral fellowship. J. C. and E. R. thank to the Generalitat de Catalunya for a Beatriu de Pinòs grant and an ICREA Academia award, respectively.

References

1- (a) J. C. Toledo Jr., O. Augusto Chem. Res. Toxicol. 2012, 25, 975-989; (b) F. Roncaroli, M. Videla, L. D. Slep, J. A. Olabe, Coord. Chem. Rev. 2007, 251, 1903-1930; (c) J. A. McCleverty, Chem. Rev. 2004, 104, 403-418.

2- N. Lehnert, W. R. Scheidt, M. W. Wolf, Struct. Bond 2014, 154, 155-224.

3- T. C. Berto, A. L. Speelman, S. Zheng, N. Lehnert, Coord. Chem Rev. 2013, 257, 244-259.

4- A. Earnshaw, E. A. King, L. F. Larkworthy, J. Chem. Soc. A 1969, 2459.

5- B. W. Fitzsimmons; L. F. Larkworthy, K. A. Rogers Inorg. Chim Acta **1980**, 44, L53-L54.

6- Numata, Y.; Kubokura, K.; Nonaka, Y.; Okawa, H.; Kida, S. Inorg. Chim. Acta 1980, 43, 193.

7- B. Weber, H. Görls, M. Rudolph, E. G. Jäger, Inorg. Chim. Acta 2002, 337, 247-265.

8- K. D. Hodges, R. G. Wollmann, S. L. Kessel, D. N. Hendrickson, D. G. Van Derveer, E. K. Barefield, *J. Am. Chem. Soc*. 1979, 101, 906-917.

9- M Li, D. Bonnet, E. Bill, F. Neese, T. Weyhermüller, N. Blum, D. Sellmann, K. Wieghardt, Inorg. Chem. 2002, 41, 3444-3456.

10- J. H. Enemark, R. D. Feltham Coord. Chem. Rev. 1974, 13, 339-406.

11- D. M. P. Mingos, Struct. Bond. 2014, 153, 1-44.

12- C. A. Brown; M. A. Pavlosky, T. E. Westre, Y. Zhang, B. Hedman, K. O. Hodgson, E. I. Solomon, J. Am. Chem. Soc. 1995, 117, 715-732.

13- N. Sun, L. V. Liu, A. Dey, G. Villar-Acevedo, J. A. Kovacs, M. Y. Darensbourg, K. O. Hodgson, B. Hedman, E. I. Solomon, Inorg. Chem. 2011, 50, 427-436.

14- a) Y. Zhang, E. Oldfield J. Phys. Chem. A 2003, 107, 4141-4150; b) Y. Zhang, E. Oldfield J. Am. Chem. Soc. 2004, 126, 9494-9495.

15- S. Chakraborty, J. Reed, M. Ross, M. J. Nilges, I. D. Petrik, S. Ghosh, S. Hammes-Schiffer, J. T. Sage, Y. Zhang, C. E. Schulz, Y. Lu, Angew. Chem. Int. Ed. 2014, 53, 2417 –2421.

16- N. Ortega-Villar, A. L. Thompson, M. C. Muñoz, V. M. Ugalde-Saldívar, A. E. Goeta, R. Moreno-Esparza, J. A. Real Chem. Eur. J. 2005, 11, 5721-5734.

17- N. Ortega-Villar, A. Y. Guerrero-Estrada, L. Piñeiro-López, M. C. Muñoz, M. Flores-Álamo, R. Moreno-Esparza, J. A. Real, V**.** M. Ugalde-Saldívar Inorg. Chem. 2015, 54, 3413-3421.

18- T. Nebe, A. Beitat, C. Würtele, C. Dücker-Benfer, R. van Eldik, C. J. McKenzie, S. Schindler, Dalton Trans. 2010, 39, 7768-7773.

19- (a) O. Kahn in "Molecular Magnetism", 1993 VCH Publishers, Inc.; (b) C. P. Slichter and H. G. Drickamer, *J. Chem. Phys*., 1972, **56**, 2142-2161.

20- N. C. Tomson, M. R. Crimmin, T. Petrenko, L. E. Rosebrugh, S. Sproules, W. C. Boyd, R. G. Bergman, S. DeBeer, F. D. Toste, K. Wieghardt, *J. Am. Chem. Soc*. 2011, 133, 18785-18801.

21- M. Sorai, *Top. Curr. Chem*., 2004, 235, 153-170.

22- P. J. van Koningsbruggen, Y. Maeda, H. Oshio, *Top. Curr. Chem*., 2004, 233, 259-324.

23- H. A. Goodwin, *Top. Curr. Chem*., 2004, 234, 23-47.

24- M. Schmitz, M. Seibel, H. Kelm, S. Demeshko, F. Meyer, H. J. Krüger, *Angew. Chem. Int. Ed.* 2014, 53, 1-6.

25- H. Chun, E. Bill, T. Weyhermüller, K. Wieghardt, *Inorg. Chem*. 2003, 42, 5612-5620.

26- F. V. Wells, S. W. McCann, H. H. Wickman, S. L. Kessel, D. N. Hendrickson, R. D. Feltham, *Inorg. Chem*. 1982, 21, 2306-2311.

27- T. C. Berto, M. B. Hoffman, Y. Murata, K. B. Landenberger, E. E. Alp, J. Zhao, N. Lehnert *J. Am. Chem. Soc*. 2011, 133, 16714-16717.

28- E. Konig, J. G. Ritter, J. Dengler, L. F. Larkworthy, *Inorg. Chem*. 1992, 31, 1196-1202

29- F. V. Wells, S. W. McCann, H. H. Wickman, S. L. Kessel, D. N. Hendrickson, R. D. Feltham, *Inorg. Chem*. 1982, 21, 2306-2311.

30- A. Hauser, *J. Chem. Phys*. 1991, 94, 2741.

31- C. Hauser, T. Glaser, E. Bill, T. Weyhermüller, K. Wieghardt, *J. Am. Chem. Soc*. 2000, 122, 4352-4365.

32- V. K. K. Praneeth, F. Paulat, T. C. Berto, S. D. George, C. Näther, C. D. Sulok, N. Lehnert, J. Am. Chem. Soc. 2008, 130, 15288-15303.

33- J.A. Olabe, Dalton Trans., 2008, 3633

34- D. P. Linder, K. R. Rodgers, J. Banister, G. R. A. Wyllie, M. K. Ellison, W. R. Scheidt J. Am. Chem. Soc. 2004, 126, 14136-14148.

35- P. Gans, A. Sabatini, L. Sacconi Inorg. Chem. 1966, 5, 1877-1881

36- K. J. Haller, P. L. Johnson, R. D. Feltham, J. H. Enemark, J. R. Ferraro, L. J. Basile, Inorg. Chim. Acta 1979, 33, 119-130.

37- N. Sun, L. V. Liu, A. Dey, G. Villar-Acevedo, J. A. Kovacs, M. Y. Darensbourg, K. O. Hodgson, B. Hedman, E. I. Solomon, Inorg. Chem. 2011, 50, 427-436.

38- G. M. Sheldrick, Acta Crystallogr., Sect. A: Fundam. Crystallogr., 2008, 64, 112-121.

39- M. J. Frisch, G. W. Trucks, H. B. Schlegel, G. E. Scuseria, M. A. Robb, J. R. Cheeseman, G. Scalmani, V. Barone, B. Mennucci, G. A. Petersson, H. Nakatsuji, M. Caricato, X. Li, H. P. Hratchian, A. F. Izmaylov, J. Bloino, G. Zheng, J. L. Sonnenberg, M. Hada, M. Ehara, K. Toyota, R. Fukuda, J. Hasegawa, M. Ishida, T. Nakajima, Y. Honda, O. Kitao, H. Nakai, T. Vreven, J. A. Montgomery Jr., J. E. Peralta, F. Ogliaro, M. J. Bearpark, J. Heyd, E. N. Brothers, K. N. Kudin, V. N. Staroverov, R. Kobayashi, J. Normand, K. Raghavachari, A. P. Rendell, J. C. Burant, S. S. Iyengar, J. Tomasi, M. Cossi, N. Rega, N. J. Millam, M. Klene, J. E. Knox, J. B.

Cross, V. Bakken, C. Adamo, J. Jaramillo, R. Gomperts, R. E. Stratmann, O. Yazyev, A. J. Austin, R. Cammi, C. Pomelli, J. W. Ochterski, R. L. Martin, K. Morokuma, V. G. Zakrzewski, G. A. Voth, P. Salvador, J. J. Dannenberg, S. Dapprich, A. D. Daniels, Ö. Farkas, J. B. Foresman, J. V. Ortiz, J. Cioslowski and D. J. Fox, Gaussian, Inc., Wallingford, CT, USA, 2009.

40- V. N. Staroverov, G. E. Scuseria, J. M. Tao, J. P. Perdew, *J. Chem. Phys.*, 2003, 119, 12129-12137.

41- J. M. Tao, J. P. Perdew, V. N. Staroverov, G. E. Scuseria, *Phys. Rev. Lett.*, 2003, 91.

42- J. Cirera, F. Paesani, *Inorg. Chem.*, 2012, 51, 8194-8201.

43- K. P. Jensen, J. Cirera, *J. Phys. Chem. A*, 2009, 113, 10033-10039.

44- J. Cirera, E. Ruiz, *J. Mat. Chem. C*, 2015, 3, 7954-7961.

45- E. Ruiz, *Phys Chem Chem Phys*, 2014, 16, 14-22.

46- A. Schäfer, C. Huber, R. Ahlrichs, *J. Chem. Phys.*, 1994, 100, 5829-5835.

47- E. Ruiz, P. Alemany, S. Alvarez and J. Cano, *J. Am. Chem. Soc.*, 1997, 119, 1297-1303.

48- E. Ruiz, J. Cano, S. Alvarez and P. Alemany, *J. Comp. Chem.*, 1999, 20, 1391-1400.

49- N. Ortega-Villar, V**.** M. Ugalde-Saldívar, M. C. Muñoz, L. A. Ortiz-Frade, J. G. Alvarado-Rodríguez, J. A. Real, R. Moreno-Esparza, *Inorg. Chem*. 2007, **46**, 7285-7293.

Table 1. Crystal data of compound **1**.

Empirical formula	$C_{27}H_{29}N_6OP_2F_{12}Fe$								
Mr	799.35								
Crystal system	orthorhombic								
Space group	Pbca								
Z	8								
Crystal size (mm)	0.06 x 0.10 x 0.10								
F(000)	3240								
T / K	**120 K**	**200 K**	**250 K**	**275 K**	**300 K**	**340 K**	**380 K**	**400 K**	**420 K**
a (Å)	17.1485(3)	17.2552(2)	17.3540(5)	17.3638(2)	17.4065(4)	17.4527(2)	17.4819(5)	17.5159(3)	17.5396(4)
b (Å)	18.8049(4)	18.8664(2)	18.9388(5)	18.9585(2)	18.9710(5)	19.0622(3)	19.1080(4)	19.1566(4)	19.2019(5)
c (Å)	19.2745(4)	19.3440(2)	19.4544(5)	19.4477(2)	19.5023(5)	19.5749(2)	19.6398(5)	19.6896(3)	19.7292(4)
V (Å$_3$)	6215.6(2)	6297.31(12)	6393.9(3)	6402.05(12)	6440.0(3)	6512.33(14)	6560.6(3)	6606.8(2)	6644.7(3)
D_c (mg cm^{-3})	1.708	1.686	1.661	1.659	1.649	1.631	1.619	1.607	1.598
μ (Mo-K$_\alpha$)(mm^{-1})	0.696	0.687	0.676	0.676	0.672	0.664	0.659	0.655	0.651
No. of total reflections	8462	8475	9262	9293	8579	8941	8940	9057	9017
No. of reflections [$I>2\sigma(I)$]	4874	6568	6468	6309	5865	5669	5424	4881	4276
R_1 [$I>2\sigma(I)$]	0.0584	0.0453	0.0606	0.0651	0.0677	0.0740	0.0749	0.0930	0.1031
R_1 [all data]	0.1255	0.0638	0.0902	0.0968	0.0983	0.1140	0.1182	0.1495	0.1363
S	0.862	0.812	0.904	0.831	0.860	1.036	1.028	1.133	1.223

$R_1 = \Sigma \, ||Fo| - |Fc|| \, / \, \Sigma \, |Fo|$; $wR = [\, \Sigma \, [w(Fo^2 - Fc^2)^2] \, / \, \Sigma \, [w(Fo^2)^2]]^{1/2}$; $w = 1/ [\square^2(Fo^2) + (m\,P)^2 + n\,P]$ where $P = (Fo^2 + 2Fc^2)/3$;
m = 0.1058 (**120 K**), 0.1088 (**200 K**), 0.1355 (**250 K**), 0.1635 (**275 K**), 0.1809 (**300 K**), 0.1282 (**340 K**), 0.1316 (**380 K**), 0.2000 (**400 K**), 0.2000 (**420 K**);
n = 16.5463 (**120 K**), 12.8834 (**200 K**), 9.4233 (**250 K**), 13.1359 (**275 K**), 11.1178 (**300 K**), 7.2081 (**340 K**), 4.877 (**380 K**), 0.0000 (**400 K**), 0.0000 (**420 K**).

Table 2. Selected experimental and computed bond lengths and angles for **1**.

	Experimental										**Computed**	
	120 K S = 1/2	**200 K**	**250 K**	**275 K**	**300 K**	**340 K**	**380 K**	**400 K**	**420 K**	Extrapolated S = 3/2*	**{FeNO}$_7$□** (S= 1/2)	**{FeNO}$_7$□** (S= 3/2)
Fe-N1	1.994(3)	1.999(2)	2.012(3)	2.023(3)	2.034(3)	2.056(3)	2.072(3)	2.085(4)	2.098(7)	2.085	2.004	2.175
Fe-N2	2.100(3)	2.105(2)	2.115(2)	2.123(2)	2.138(3)	2.154(3)	2.166(3)	2.171(4)	2.190(5)	2.231	2.082	2.255
Fe-N3	1.987(3)	1.999(2)	2.014(3)	2.025(3)	2.033(3)	2.063(3)	2.078(3)	2.080(4)	2.085(7)	2.158	2.005	2.161
Fe-N4	2.084(3)	2.084(2)	2.102(2)	2.113(2)	2.128(3)	2.163(3)	2.179(3)	2.193(3)	2.203(5)	2.285	2.071	2.260
Fe-N5	1.992(3)	1.992(2)	2.007(2)	2.021(3)	2.032(3)	2.065(3)	2.087(3)	2.094(4)	2.099(6)	2.180	2.006	2.193
Fe-N6	1.733(3)	1.738(2)	1.745(3)	1.740(3)	1.745(3)	1.751(4)	1.753(3)	1.745(5)	1.751(7)	1.755	1.759	1.782
N6-O	1.170(4)	1.157(3)	1.143(4)	1.133(4)	1.126(5)	1.111(5)	1.102(5)	1.106(7)	1.099(10)	1.052	1.170	1.156
Fe-N_{bztpen}	2.031	2.036	2.050	2.061	2.073	2.100	2.116	2.125	2.135	2.204	2.034	2.209
Fe-N_{av}	1.982	1.986	1.999	2.008	2.018	2.042	2.056	2.061	2.071	2.127	1.988	2.138
Fe-N-O	144.0(3)	144.5(2)	145.8(3)	147.4(3)	148.8(4)	151.0(4)	154.7(9)	156.5(6)	157.9(10)	167	143.4	165.6
Σ	60.88	60.87	62.20	65.16	67.34	71.31	74.55	77.24	76.80	90.95	59.23	92.48
Φ	4.4	4.4	4.4	4.6	4.8	5.1	5.3	5.5	5.5	6.42	3.63	5.60

Scheme I. Ligands concerned with the synthesis of iron-nitrosyl complexes exhibiting SCO properties.

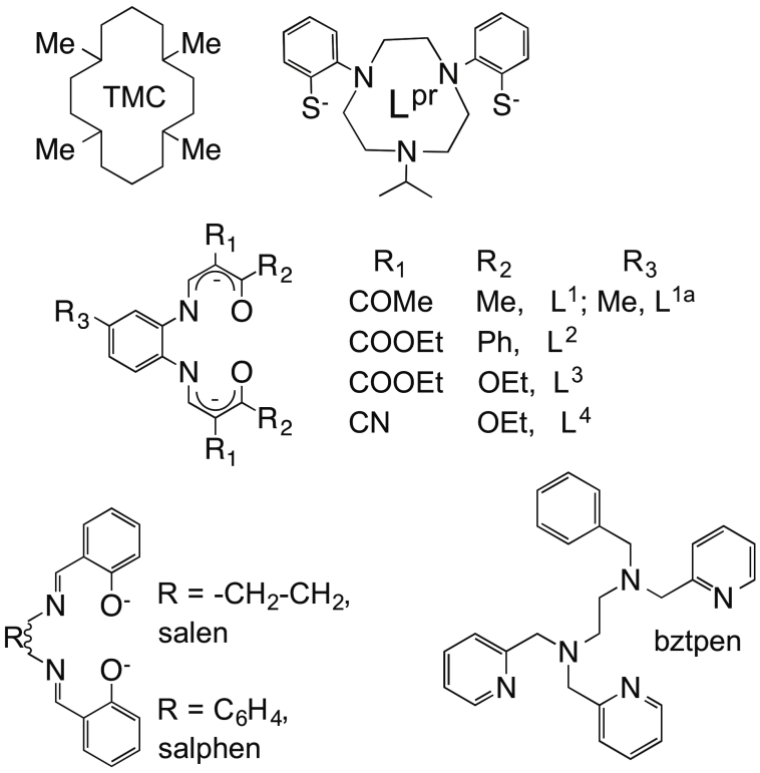

Figure captions

Figure 1. Magnetic behavior of **1** in the temperature range 2-400 K. Red line corresponds to the best fit of the experimental data (see text).

Figure 2. Spectroscopic measurements for **1**: (a) EPR spectra at 4 K and 300 K; (b) Mössbauer spectra at 293 K and 80 K; and (c) Visible spectrum at 300 K (the inset shows the thermal variation of the 555 nm peak in the temperature interval 175-425 K).

Figure 3. Correlation of magnetic (experimental and calculated) and spectroscopic (UV-VIS and Raman) data. Full squares indicate the Raman peak intensity ratio $I_{1789}/(I_{1789} + I_{1684})$ of the ν_{NO} stretching mode. Open circles show the (normalized and inversed) absorbance variation at 555 nm.

Figure 4. Representative variable-temperature (a) Raman scattering (532 nm excitation, -z(yy)z configuration) and (b) infrared absorption spectra of a single crystal of **1**.

Figure 5. Molecular structure (left) and perspective view of the crystal packing in the [100] direction (PF_{6}^{-} anions are not shown)(right) of **1**.

Figure 6. Magneto-structural correlation. (a) The thermal variation of $\chi_M T$ and average Fe-N_{av} bond length; (b) Thermal variation of the average Fe-N_{av} bond length and Fe-NO bond angle. $\chi_M T$ (black circles), Fe-N_{av} (red squares) and Fe-NO bond angle (blue squares).

Figure 7. Optimized structures (left) and spin density (right) isocontours (0.02 e/$Å^{-3}$) for the $[Fe(bztpen)(NO)]^{2+}$ molecule in the S = 3/2 state (top) and S = 1/2 (bottom).

Figure 8. Computed (red line) and experimental (open circles) magnetic behavior of **1** in the temperature range 0-1000 K. The computed equilibrium temperature $T_{1/2calc}$ at which $\Delta G = 0$ is 546 K (see text).

Figure 1

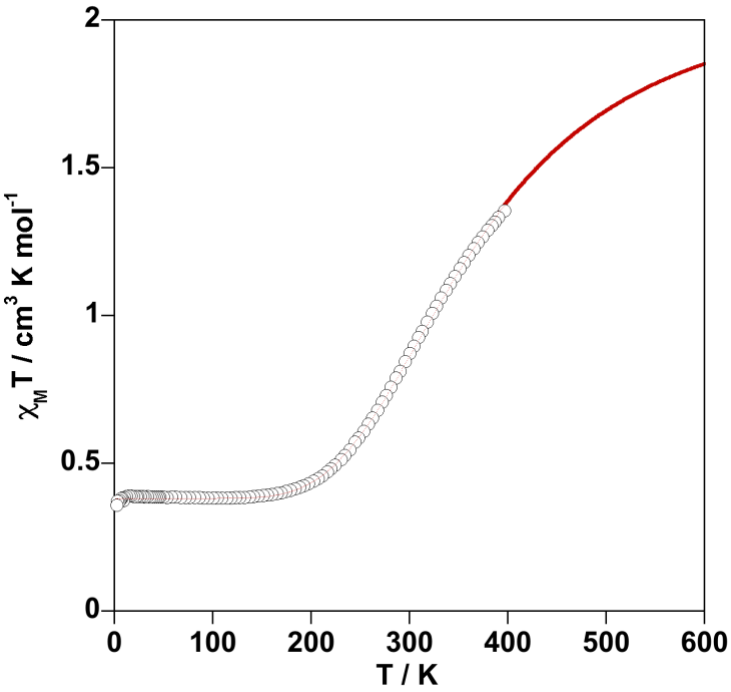

Figure 2

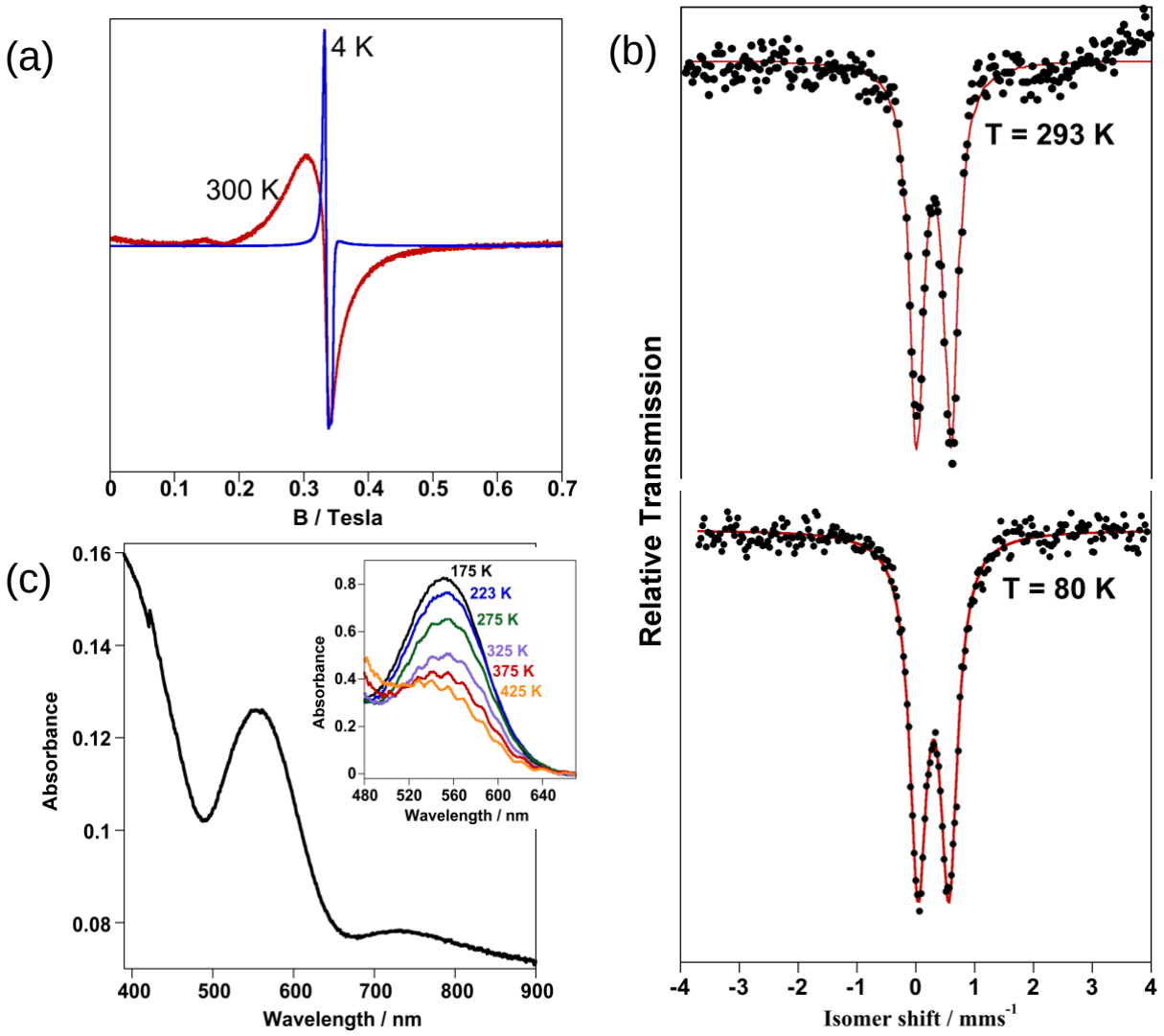
(a)
4 K
300 K
0
0.1
0.2
0.3
0.4
0.5
0.6
0.7
B / Tesla
(b)
T = 293 K
T = 80 K
Relative Transmission
-4
-3
-2
-1
0
1
2
3
4
Isomer shift / mms-1
(c)
Absorbance
0.16
0.14
0.12
0.1
0.08
400
500
600
700
800
900
Wavelength / nm
175 K
223 K
275 K
325 K
375 K
425 K
0.8
0.6
0.4
0.2
0
480
520
560
600
640
Wavelength / nm

Figure 3

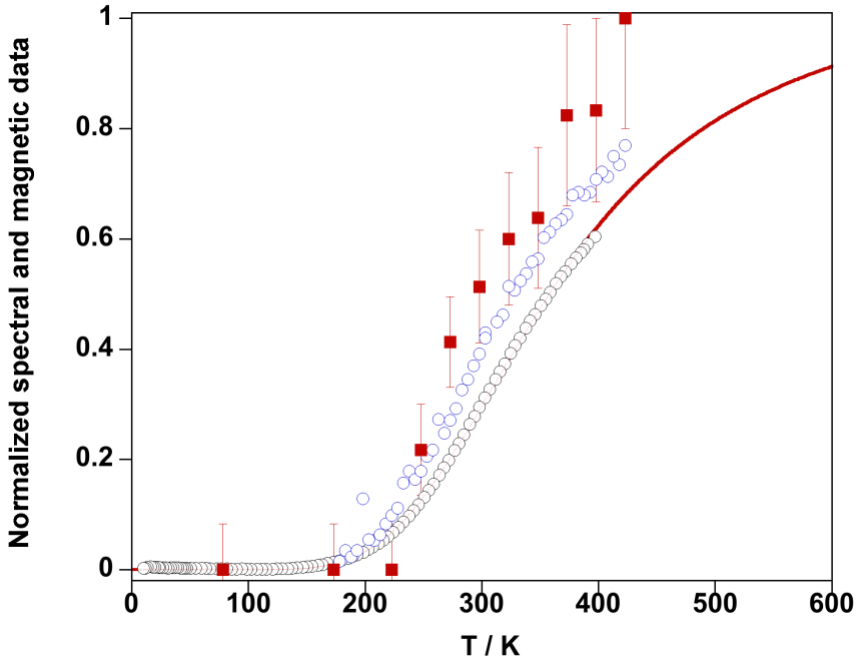
Normalized spectral and magnetic data
1
0.8
0.6
0.4
0.2
0
0
100
200
300
400
500
600
T / K

Figure 4

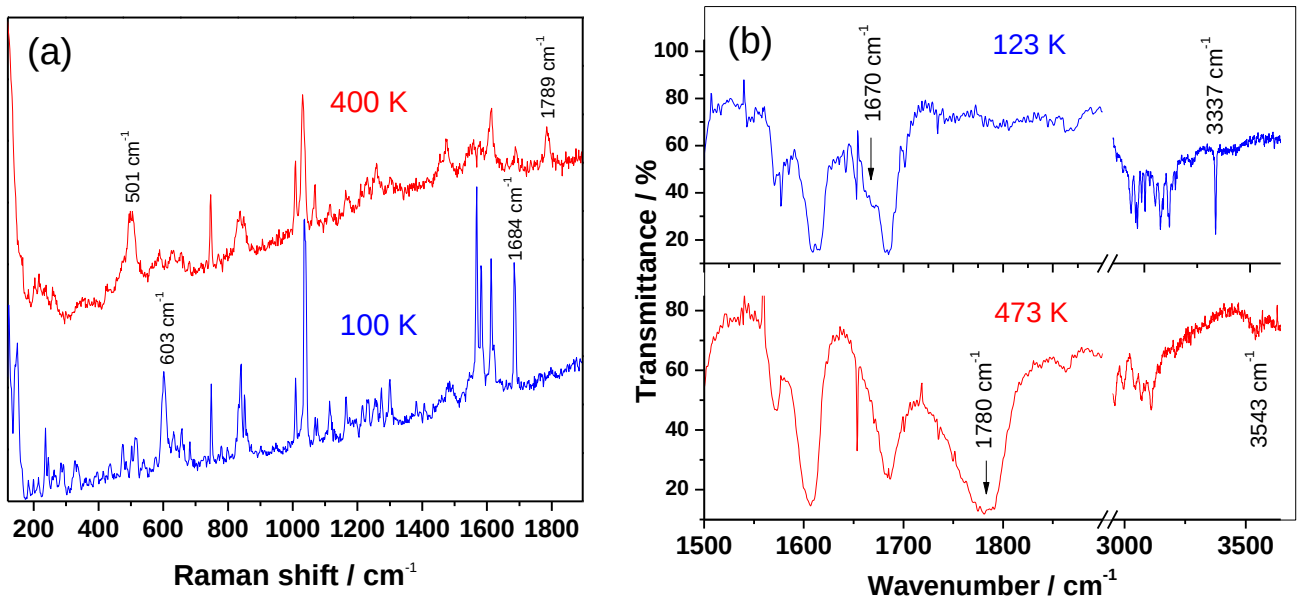
(a)
400 K
100 K
501 cm-1
603 cm-1
1684 cm-1
1789 cm-1
200 400 600 800 1000 1200 1400 1600 1800
Raman shift / cm-1
(b)
123 K
473 K
1670 cm-1
3337 cm-1
1780 cm-1
3543 cm-1
Transmittance / %
100 80 60 40 20
1500 1600 1700 1800 3000 3500
Wavenumber / cm-1

Figure 5

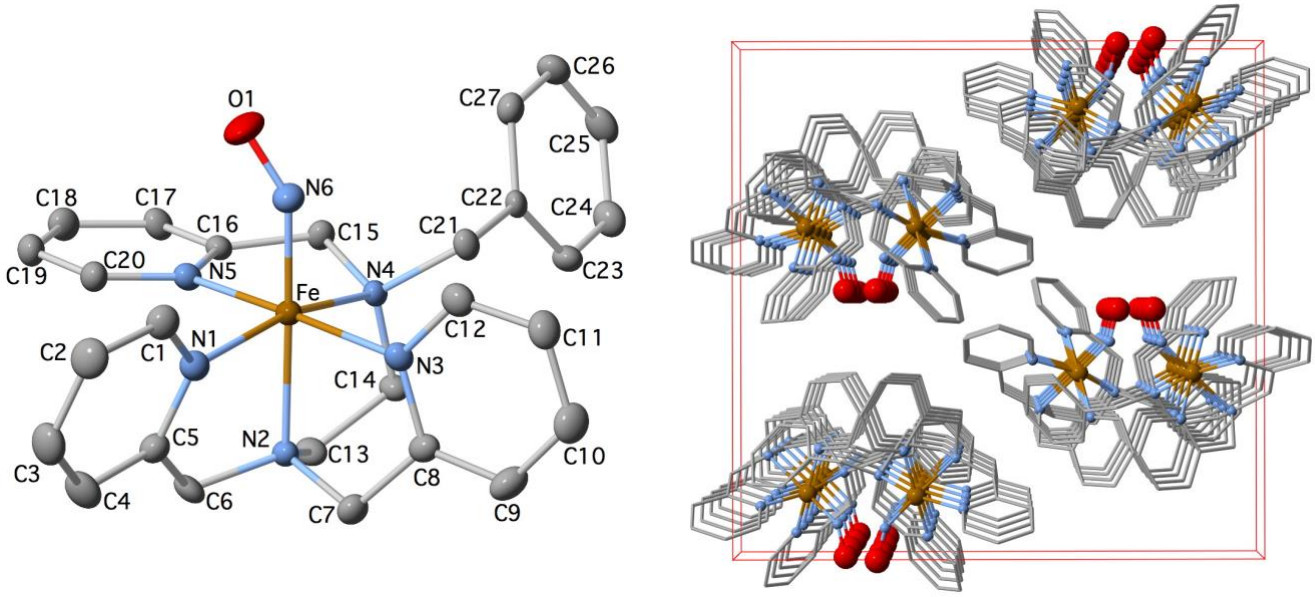
O1
N6
C26
C27
C25
C18
C17
C16
C15
C22
C24
C21
C19
C20
N5
N4
C23
Fe
C12
C11
C2
C1
N1
N3
C14
C5
N2
C13
C10
C3
C8
C4
C6
C7
C9

Figure 6

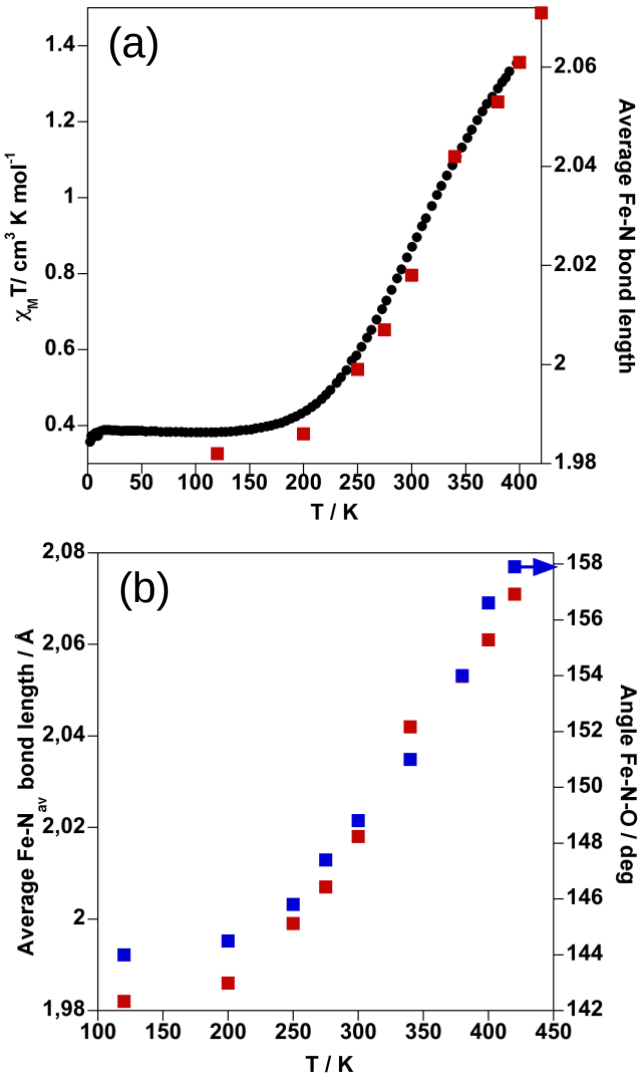
(a)
1.4
1.2
1
0.8
0.6
0.4
χ_MT/ cm^3 K mol^{-1}
0
50
100
150
200
250
300
350
400
T / K
2.06
2.04
2.02
2
1.98
Average Fe-N bond length
(b)
2,08
2,06
2,04
2,02
2
1,98
Average Fe-N$_{av}$ bond length / Å
100
150
200
250
300
350
400
450
T / K
158
156
154
152
150
148
146
144
142
Angle Fe-N-O / deg

Figure 7

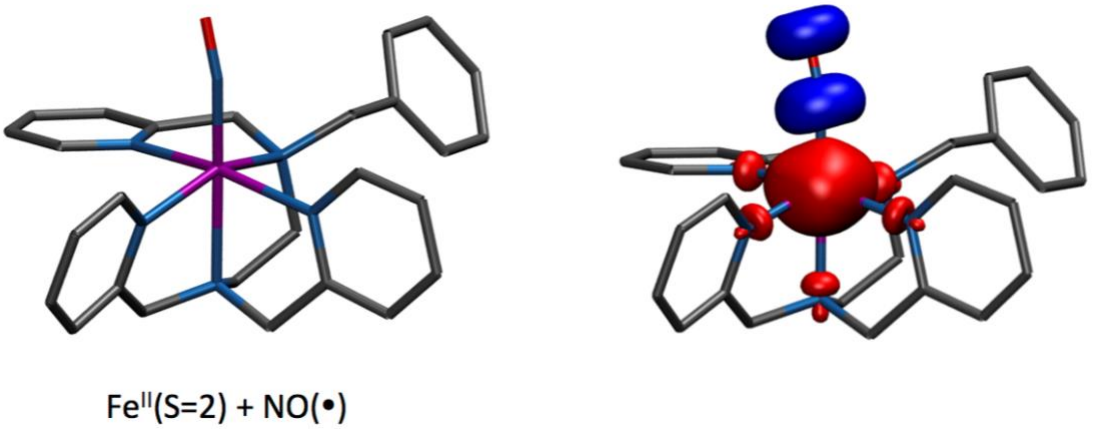

$Fe^{II}(S=2) + NO(\bullet)$

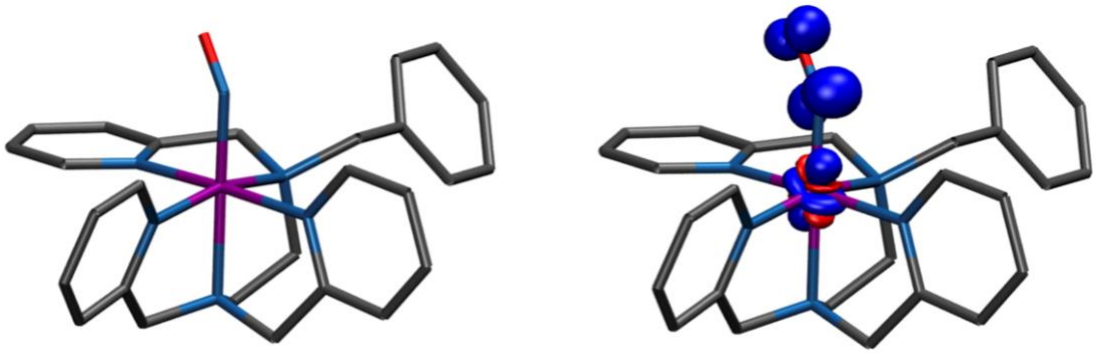

$Fe^{II}(S=0) + NO(\bullet)$

Figure 8

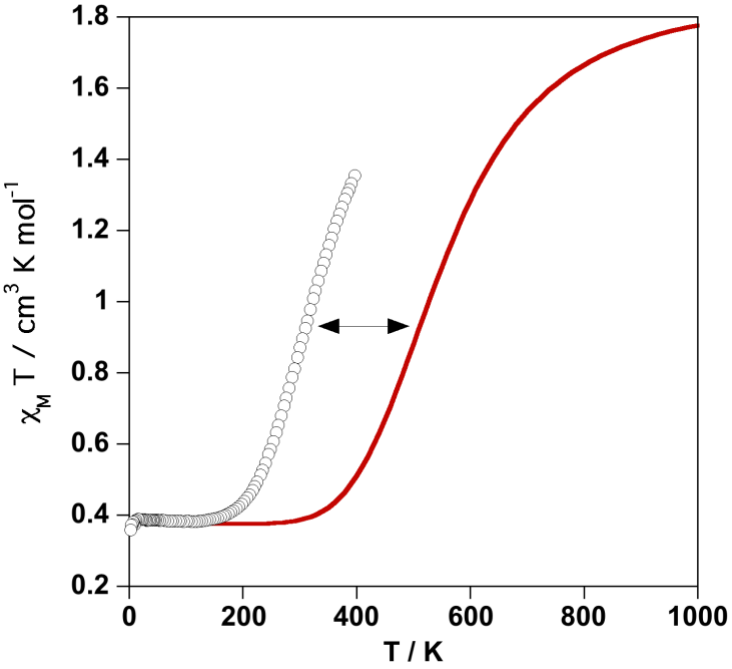

Supporting Information

Table S1. ^{57}Fe Mössbauer data for **1** δ (isomer shift), ΔE_Q (quadrupolar splitting), A (……) and w+ (…..) obtained from metallic α-Fe reference.

	CS (vs. α Fe)	**Δ**	**A**	**w+**	
Doublet 80 K	0.3060(50)	0.5231(86)	47500(1200)	0.1749(67)	**(mm/s)**
	CS (vs. α Fe)	**Δ**	**A**	**w+**	
Doublet 293 K	0.2954(45)	0.5905(83)	100500(2800)	0.1458(59)	**(mm/s)**

Figure S1. Photographs of a crystalline sample of **1** at ….K (left) and at …..K (right) showing the change of color upon SCO.

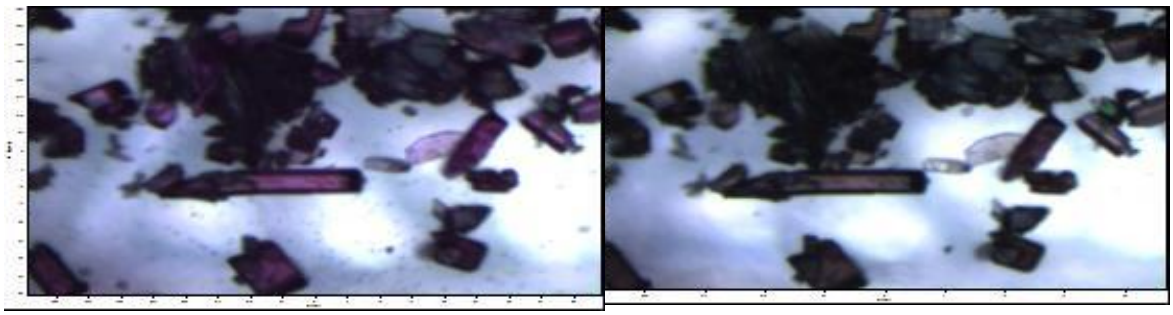

Figure S2. Intermolecular interactions between complex cations.

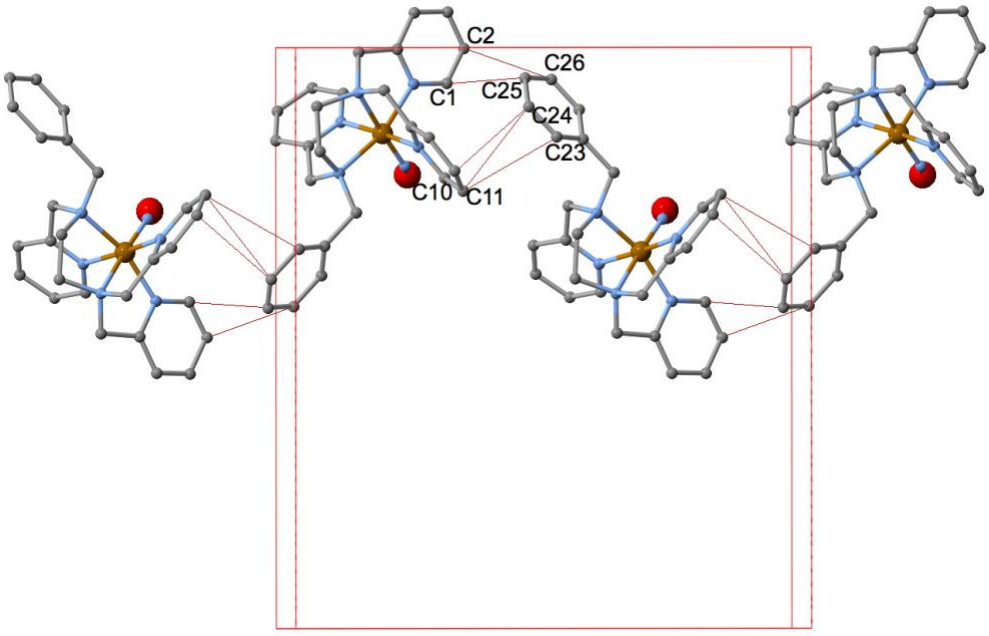

Table S2. Intermolecular C···C and C···F contacts.

T / K	**120**	**200**	**250**	**275**	**300**	**340**	**380**	**400**
C(1)···C(25)$_{i}$	3.641(6)	3.674(4)	3.714(5)	3.712(6)	3.729(6)	3.761(7)	3.781(7)	3.84(2)
C(2)···C(26)$_{i}$	3.600(6)	3.624(4)	3.652(6)	3.661(6)	3.675(7)	3.719(8)	3.749(8)	3.77(2)
C(10)···C(24)$_{i}$	3.645(6)	3.657(4)	3.698(6)	3.705(6)	3.714(7)	3.753(8)	3.778(8)	3.84(2)
C(11)···C(23)$_{i}$	3.652(6)	3.685(4)	3.719(5)	3.733(6)	3.748(6)	3.759(7)	3.772(7)	3.834(14)
C(11)···C(24)$_{i}$	3.588(6)	3.593(4)	3.612(5)	3.618(6)	3.628(6)	3.658(7)	3.667(7)	3.679(14)
C(13)···C(25)$_{ii}$	3.616(6)	3.638(4)	3.664(5)	3.680(5)	3.699(5)	3.740(6)	3.788(6)	3.813(13)
C(19)···C(19)$_{iii}$	3.572(6)	3.574(4)	3.580(5)	3.574(5)	3.584(6)	3.599(7)	3.614(7)	3.601(14)
C(2)···F(1)$_{iv}$	3.112(5)	3.145(4)	3.184(5)	3.187(6)	3.201(6)	3.229(7)	3.233(7)	3.270(14)
C(7)···F(11)	3.146(5)	3.184(4)	3.214(6)	3.222(6)	3.233(7)	3.278(9)	3.316(10)	3.399(13)
C(13)···F(2)	3.163(5)	3.171(3)	3.191(4)	3.198(4)	3.209(5)	3.232(5)	3.247(5)	3.277(10)
C(14)···F(2)	3.078(5)	3.109(3)	3.154(4)	3.158(4)	3.178(5)	3.217(5)	3.232(5)	3.257(10)
C(15)···F(4)	3.133(4)	3.143(3)	3.172(4)	3.181(4)	3.194(4)	3.217(5)	3.235(5)	3.252(10)
C(15)···F(5)	3.163(5)	3.180(3)	3.201(4)	3.207(5)	3.220(5)	3.233(5)	3.252(5)	3.283(10)
C(17)···F(4)	3.142(4)	3.159(3)	3.185(4)	3.183(4)	3.194(4)	3.209(5)	3.223(5)	3.247(10)
C(17)···F(6)	3.144(5)	3.173(3)	3.205(4)	3.216(5)	3.221(5)	3.265(6)	3.299(6)	3.352(13)
C(17)···F(12)$_{iii}$	3.000(5)	3.035(3)	3.074(5)	3.081(5)	3.094(6)	3.118(7)	3.143(7)	3.155(12)
C(18)···F(12)$_{iii}$	3.068(5)	3.083(4)	3.095(5)	3.095(6)	3.095(6)	3.121(7)	3.135(7)	3.171(13)
C(19)···F(12)	3.097(5)	3.121(3)	3.157(5)	3.171(5)	3.185(6)	3.219(7)	3.233(7)	3.314(12)
C(20)···F(12)	3.122(5)	3.157(3)	3.195(4)	3.199(5)	3.214(5)	3.243(6)	3.271(6)	3.332(12)

i = x+1/2, y, -z+1/2; ii = x, -y+3/2, z+1/2; iii = -x+1, -y+1, -z+1; iv = -x+1, y-1/2, -z+1/2;
iv = x+1/2, y, -z+3/2; v = -x+3/2, y+1/2, z; vi = x, -y+3/2, z-1/2

Table S3. Cartesian atomic coordinates for the optimized geometries.

S1.1. *[Fe(bztpen)(NO)]$^{2+}$ S = 1/2, E= -2713.94483906 au, ν_1 = 21.0953 cm^{-1}*

Fe	-0.041534	0.659053	-0.357101
N	0.227161	2.644857	-0.387026
N	0.328329	0.992216	1.664010
N	1.949305	0.432061	-0.433460
N	-0.366013	-1.310941	0.191479
N	-2.028060	0.809281	-0.126519
N	-0.296384	0.415456	-2.080215
O	-1.112593	0.181564	-2.884902
C	0.530777	3.388330	-1.468630
C	0.746520	4.756073	-1.390931
C	0.658331	5.383582	-0.152793
C	0.359176	4.616783	0.970362
C	0.144590	3.253510	0.822503
C	-0.228174	2.339162	1.959981
C	1.803528	0.975182	1.932611
C	2.615834	0.578649	0.727992
C	3.996083	0.418824	0.808628
C	4.713557	0.115949	-0.341255
C	4.025925	-0.013670	-1.545536
C	2.651660	0.146855	-1.550931
C	-0.373959	-0.111793	2.375171
C	-0.038621	-1.403516	1.656119
C	-1.812849	-1.593175	-0.053334
C	-2.662147	-0.366663	0.079165
C	-4.035643	-0.436705	0.285241
C	-4.789626	0.729358	0.243910
C	-4.143220	1.935243	-0.013201
C	-2.769897	1.935986	-0.188257
C	0.460709	-2.351067	-0.567709
C	0.155226	-3.791960	-0.239565
C	0.806198	-4.443869	0.815159
C	0.532750	-5.777887	1.101001
C	-0.387136	-6.482180	0.327229
C	-1.021031	-5.853462	-0.741842
C	-0.748056	-4.518605	-1.024742
H	0.597021	2.859645	-2.410872
H	0.982250	5.311729	-2.289702
H	0.826903	6.449893	-0.060163
H	0.292350	5.070243	1.952261
H	-1.315009	2.246617	2.022217
H	0.128085	2.724447	2.920063
H	2.111345	1.976454	2.244978
H	2.015287	0.309753	2.774422
H	4.498715	0.537916	1.761590
H	5.788865	-0.010735	-0.300748
H	4.542294	-0.241506	-2.469354
H	2.073787	0.047728	-2.460593
H	-0.068085	-0.168391	3.425521
H	-1.443259	0.096996	2.348120
H	-0.550310	-2.256387	2.108373
H	1.033845	-1.593751	1.727215
H	-1.902433	-1.942270	-1.085768
H	-2.163743	-2.406901	0.585484
H	-4.504403	-1.397840	0.459467
H	-5.862015	0.696950	0.395361

H	-4.690962	2.866791	-0.077404
H	-2.235092	2.853193	-0.390916
H	0.279218	-2.158646	-1.625918
H	1.501992	-2.118947	-0.349778
H	1.554619	-3.919655	1.401975
H	1.050188	-6.273244	1.914218
H	-0.592432	-7.524010	0.543212
H	-1.713659	-6.406782	-1.365099
H	-1.220560	-4.050974	-1.883924

S1.2. *[Fe(bztpen)(NO)]$^{2+}$ S = 3/2, E=-2713.93366629 au, ν_1 = 21.2625 cm^{-1}*

Fe	-0.007656	-0.725660	-0.616869
N	-0.174232	-2.883405	-0.398227
N	-0.365026	-1.047485	1.585934
N	-2.138194	-0.396000	-0.460740
N	0.391727	1.371342	0.126116
N	2.151065	-0.774196	-0.236188
N	0.236852	-0.546433	-2.372544
O	0.675121	-0.454953	-3.438645
C	-0.435756	-3.743215	-1.401993
C	-0.593502	-5.105003	-1.195655
C	-0.480858	-5.600935	0.099644
C	-0.219180	-4.715720	1.142055
C	-0.067904	-3.363558	0.861111
C	0.264598	-2.345291	1.925985
C	-1.828426	-1.109246	1.855681
C	-2.691712	-0.533845	0.758039
C	-4.034337	-0.245267	0.989257
C	-4.830490	0.174307	-0.069193
C	-4.262569	0.294466	-1.336113
C	-2.917356	0.008890	-1.486749
C	0.285414	0.097815	2.274722
C	-0.043710	1.394590	1.554165
C	1.850176	1.633065	-0.004261
C	2.713343	0.402795	0.098965
C	4.065470	0.502228	0.418341
C	4.863888	-0.632960	0.358737
C	4.287746	-1.842304	-0.023590
C	2.932429	-1.871636	-0.304801
C	-0.371286	2.428904	-0.661437
C	-0.094746	3.862648	-0.276137
C	0.851395	4.612940	-0.984137
C	1.106019	5.938427	-0.644837
C	0.411224	6.533634	0.405174
C	-0.549838	5.805276	1.102936
C	-0.804781	4.480891	0.760292
H	-0.519402	-3.315634	-2.393914
H	-0.802220	-5.757291	-2.034120
H	-0.602257	-6.659527	0.297409
H	-0.134299	-5.069483	2.162887
H	1.346487	-2.194721	1.956814
H	-0.044973	-2.703710	2.913570
H	-2.058274	-0.626849	2.811444
H	-2.105781	-2.162175	1.963620
H	-4.449289	-0.357565	1.984327
H	-5.878649	0.399597	0.089138
H	-4.847653	0.611094	-2.190117
H	-2.430151	0.102369	-2.449755
H	-0.039501	0.165348	3.319777

H	1.360877	-0.082341	2.277079
H	0.407863	2.241862	2.079096
H	-1.123932	1.553088	1.557101
H	2.172715	2.395702	0.710447
H	2.013956	2.055450	-0.999836
H	4.483947	1.462335	0.696708
H	5.919452	-0.574720	0.596906
H	4.874961	-2.748618	-0.099688
H	2.441470	-2.790569	-0.599135
H	-0.112179	2.268357	-1.709949
H	-1.427656	2.194229	-0.530897
H	1.373995	4.171429	-1.828178
H	1.833023	6.510460	-1.209340
H	0.602530	7.567997	0.665384
H	-1.112499	6.274663	1.901461
H	-1.582609	3.937472	1.288403

S1.3. *[Fe(bztpen)(NO)]$^{2+}$ S = 5/2, E=-2713.90128732 au, ν_1 = 22.5178 cm^{-1}*

Fe	-0.013756	-0.706622	-0.512071
N	-0.186104	-2.877874	-0.360130
N	-0.390174	-1.054085	1.629288
N	-2.135359	-0.408097	-0.464364
N	0.397560	1.390008	0.190608
N	2.147727	-0.728426	-0.286446
N	0.267905	-0.644390	-2.536271
O	0.857722	-0.700034	-3.535802
C	-0.443508	-3.729035	-1.371470
C	-0.590820	-5.093968	-1.177022
C	-0.476495	-5.600058	0.114302
C	-0.223579	-4.722556	1.165540
C	-0.080130	-3.367450	0.895650
C	0.240699	-2.353025	1.968923
C	-1.860827	-1.113138	1.867530
C	-2.706346	-0.544928	0.748197
C	-4.053172	-0.260509	0.957691
C	-4.834642	0.153499	-0.114296
C	-4.248852	0.272449	-1.372962
C	-2.900445	-0.009736	-1.502583
C	0.253338	0.094150	2.325080
C	-0.071180	1.396705	1.608807
C	1.857541	1.663080	0.094827
C	2.718463	0.426180	0.109597
C	4.075328	0.504418	0.415555
C	4.869079	-0.627321	0.283067
C	4.283776	-1.813081	-0.156956
C	2.925985	-1.823354	-0.423238
C	-0.361864	2.432217	-0.619326
C	-0.085263	3.872750	-0.261053
C	0.838489	4.617162	-1.003625
C	1.097708	5.947624	-0.687539
C	0.429714	6.553248	0.373679
C	-0.509621	5.830378	1.105994
C	-0.769414	4.501066	0.786753
H	-0.531527	-3.290527	-2.358462
H	-0.794603	-5.740837	-2.020871
H	-0.591219	-6.661111	0.302643
H	-0.139747	-5.085006	2.183383
H	1.322043	-2.196942	2.006977
H	-0.074672	-2.716043	2.952853

H	-2.109593	-0.623031	2.814378
H	-2.138505	-2.165575	1.978441
H	-4.483654	-0.370518	1.946408
H	-5.885759	0.375709	0.027988
H	-4.822566	0.584917	-2.236134
H	-2.398360	0.081795	-2.458602
H	-0.077836	0.154952	3.368349
H	1.329575	-0.085093	2.331373
H	0.362492	2.240390	2.154212
H	-1.152544	1.546605	1.589342
H	2.174090	2.366680	0.870026
H	2.032630	2.164134	-0.860943
H	4.500537	1.446655	0.740989
H	5.927883	-0.584953	0.509912
H	4.867156	-2.715393	-0.289262
H	2.428352	-2.723603	-0.760946
H	-0.097214	2.250389	-1.663609
H	-1.419077	2.199529	-0.490030
H	1.339163	4.166597	-1.856326
H	1.807368	6.514829	-1.278354
H	0.624503	7.591228	0.616281
H	-1.052040	6.307796	1.913730
H	-1.531501	3.962535	1.341997

Figure S3. Molecular orbital diagram of **1** including de relevant d-based MOs.

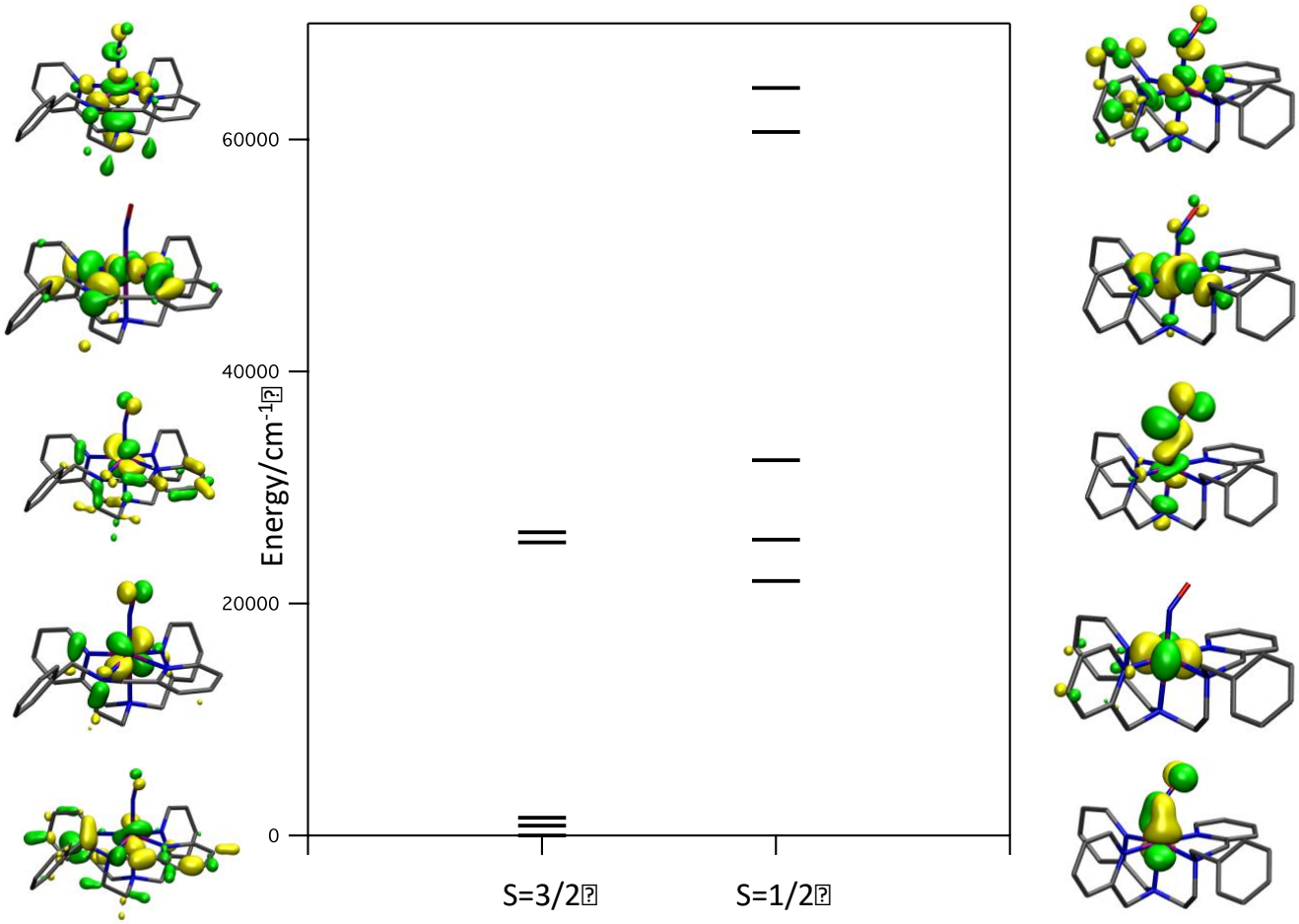

Modeling SCO in the [Fe(bztpen)(NO)]$^{2+}$ molecule.

To model the transition temperature in the [Fe(bztpen)(NO)]$^{2+}$ spin-crossover system, we used the fact that the spin-crossover phenomenon can be described as a thermodynamic equilibrium between the high-spin and the low-spin. The Gibbs free energy change (□G) associated with this process corresponds to:

$$\Delta G = G^{HS} - G^{LS} = \Delta H - T\Delta S \quad [1]$$

where

$$G^i = H^i - TS^i = E^i_{el} + E^i_{vib} - TS^i \quad [2]$$

is the Gibbs free energy associated with spin state *i*. The enthalpy term (H_i) includes both electronic (E^i_{el}) and vibrational (E^i_{vib}) contributions. For molecular complexes, E^i_{vib} can be properly estimated using the harmonic approximation, while the term E^i_{el}, describing the electronic energy of spin state *i*, can be obtained directly from *ab initio* calculations, in this case, at Density Functional Theory (DFT) level. The entropy contribution to the free energy (S_i) can also be estimated using the harmonic approximation.

Using the equilibrium constant, we can write down the corresponding molar fractions of each spin-state as follows,

$$\Delta G(T) = -RT\ln K_{eq} = -RT\ln\frac{\gamma_{HS}}{\gamma_{LS}} = -RT\ln\frac{\gamma_{HS}}{1-\gamma_{HS}} \quad [3]$$

that can be rewritten as,

$$\gamma_{HS}(T) = \left[1 + e^{\Delta G(T)/RT}\right]^{-1} \quad [4]$$

where R is the gas constant and T the temperature. This last expression provides with the molar fraction of the high-spin state at each temperature, which can be used to compute magnetic susceptibility as follows. From the molar fraction, one can estimate the magnetic moment using the spin only formula, and if the Curie law holds, from that quantity we can extract the magnetic susceptibility.

$$\mu_{eff}(T) = g_{HS}(T)\mu_{eff}(S = 3/2) + g_{LS}(T)\mu_{eff}(S = 1/2) \quad [5]$$

$$\mu_{eff}(T) = C\sqrt{c_M T} \approx 2.82787\sqrt{c_M T} \quad [6]$$

Equation 6 can be recast as,

$$c_M T = \left(\frac{\mu_{eff}(T)}{2.82787}\right)^2 \quad [7]$$

Which already provides with the temperature dependence of the magnetic susceptibility